Metrol. Meas. Syst., Vol. 32 (2025), No. 1
DOI: 10.24425/mms.2025.152777

METROLOGY AND MEASUREMENT SYSTEMS
Index 330930, ISSN 0860-8229
www.metrology.wat.edu.pl

NONDESTRUCTIVE DETECTION OF CERAMIC BALL SURFACE DEFECTS BASED ON IMPROVED YOLOv8

Guo-Qing Gu[1)], Han-Lei Wang[2)], Xu-Yi Miao[2)], Jing-Yi Yan[3)], Jian-Zhou Du[4)]

1) *School of Civil Engineering, Yancheng Institute of Technology, Yancheng 224051, China* (✉ *gqgu@ycit.edu.cn*)
2) *School of Information Engineering, Yancheng Institute of Technology, Yancheng 224051, China*
3) *Jiangsu Dongpu Fine Ceramic Technology Co. Ltd, Lianyungang 222000, China*
4) *School of Materials Science and Engineering, Yancheng Institute of Technology, Yancheng 224051, China*

Abstract

To address issues such as severe specular reflection, low detection accuracy, and large model parameters in ceramic balls detection, an improved YOLOv8 model, named YOLOv8-AP, is proposed for ceramic ball surface defects detection. Firstly, the coaxial light source is employed to reduce the specular reflection effect and an efficient image acquisition platform is established to obtain defect samples. Additionally, various data augmentation techniques are utilized to expand the dataset, and both the ADown module and an improved Powerful-IoU loss function are introduced to optimize the YOLOv8 network, significantly enhancing the detection efficiency for small target defects. Experimental results show that the proposed improved YOLOv8-AP model can achieve a mean average precision of 96.1% for the detection of the ceramic ball surface defects, which greatly enhance the defect detection accuracy compared to the traditional models and can hope to meet the intelligent and automatic detection requirements of the ceramic balls' online detection applications.

Keywords: Defect detection, ceramic ball, YOLOv8-AP model, Powerful-IoU loss function.

1. Introduction

Silicon nitride (Si_3N_4) or zirconia oxide (ZrO_2) ceramic balls exhibit exceptional properties such as high hardness, high temperature resistance, and self-lubrication [1, 2], making them widely used in key components of military equipment and new energy vehicles [3, 4]. However, due to the low brittleness of ceramic materials and the limitations of processing technology, defects such as pits, scratches, and pores easily form on their surfaces during manufacturing. These defects significantly reduce the lubrication capability and service life of ceramic balls [5]. To ensure the safety and reliability of equipment, it is crucial to study the formation and detection techniques of surface defects in ceramic balls. Manual visual inspection suffers from low accuracy and high randomness [6, 7], prompting researchers to explore other methods such as radiography, fluorescent penetrant testing, and ultrasound [8]. Although these methods have achieved certain progress, each has limitations. For example, radiographic testing can only detect larger cracks and inclusions, laser scattering methods have high misjudgement rates and costs, and fluorescent penetrant testing is effective only for open defects and is less sensitive to colour differences and shallow pits, also being relatively costly. Traditional image processing requires complex feature design to identify different defects but is less adaptable to actual production environments.

In recent years, researchers worldwide have applied machine vision for ceramic ball defect detection. Li *et al.* [9] proposed a multi-view surface defect detection method for Si_3N_4 ceramic bearing balls by enhancing features with Gabor saliency domain fusion, addressing issues of insufficient boundary, colour, and shape feature fusion due to single view limitations. Zhang *et*

Article history: received June 31, 2024; revised September 30, 2024; accepted October 24, 2024; available online January 24, 2025.

al. [10] discovered that some defects in Si_3N_4 ceramic balls could not be directly detected and proposed a surface defect detection method based on fringe reflection. By projecting sinusoidal fringes onto the Si_3N_4 ceramic balls, uniform fringes were formed on defect-free surfaces, validating the effectiveness of the method through experiments.

With the development of artificial intelligence, machine vision technology based on deep learning has made significant progress in surface defect detection in terms of speed and accuracy using convolutional neural network models. Yu *et al.* [11] proposed a defect detection algorithm based on SWT and nonlinear enhancement, solving the problem of uneven backgrounds by using low-pass filtering in the frequency domain to correct decomposition coefficients, effectively identifying surface defects in Si_3N_4 ceramic balls. Chen *et al.* [12] addressed the problem of missed detections of aluminium tube surface defects by proposing a detection method based on Faster RCNN, achieving higher recognition speed and accuracy. Liao *et al.* [13] integrated the BiFPN module in-to the neck of the YOLOv5 algorithm and proposed an improved YOLOv5-based nondestructive detection method for Si_3N_4 bearing balls, achieving good detection results. Fan *et al.* [14] designed a lightweight CM-YOLOv8 algorithm specifically for coal mining operations, significantly reducing computational requirements and model size while maintaining high precision. Likewise, Lv *et al.* [15] proposed an improved YOLOv5 method by introducing CA mechanism for milling surface roughness detection, and realized a higher detection speed and robustness to lighting environment.

Despite these advancements, challenges such as severe specular reflection, small sample sizes and low detection accuracy remain in the research on surface defect detection of ceramic balls. To address these problems, an improved YOLOv8 method, named YOLOv8-AP, is proposed for ceramic ball surface defects detection in this paper. Firstly, a vision acquisition platform is built to collect samples of surface defects on ceramic ball, and data augmentation is applied to these samples [16]; then, a ceramic ball defect dataset is created. Finally, the ADown module is introduced to replace the convolution module in the YOLOv8 model, and the Powerful-IoU loss function is also integrated to reduce computational complexity while improving detection accuracy. This ensures the extraction of small defect features in ceramic ball images, enhancing the model's detection efficiency.

2. Image Pre-processing

The dataset used in this paper is a self-constructed Si_3N_4 ceramic ball (black colour) and ZrO_2 ceramic ball (white colour) dataset. Since the quality of the dataset significantly impacts defect detection results, it is essential to build a collection device tailored to the dataset's specific characteristics to enhance sample quality. Data augmentation is employed to generate new samples, which, on one hand, increases the dataset's diversity, thereby improving the model's generalization ability; on the other hand, it introduces noise into the original data, enhancing the model's robustness [17].

2.1. Image Acquisition

To obtain high quality images of surface defects on ceramic balls, a dedicated image acquisition platform was constructed, as shown in Fig. 1. Considering the spherical nature of the subject and the significant impact of specular reflection on the captured images, a coaxial light source [18, 19] was employed for the setup. The coaxial light source is fixed directly above the ceramic ball, and the industrial camera is positioned directly above the coaxial light source, ensuring that the industrial camera, coaxial light source, and ceramic ball are aligned on a central axis.

Metrol. Meas. Syst., Vol. 32 (2025), No. 1
DOI: 10.24425/mms.2025.152777

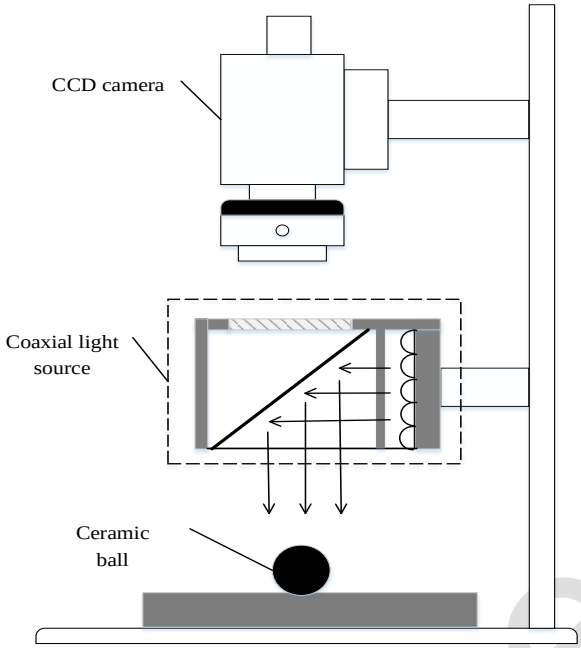

Fig. 1. The schematic for image acquisition platform.

The coaxial light source enables light to illuminate directly onto the detected object, almost parallel to the imaging axis, which is crucial for minimizing shadows and reflections on reflective surfaces such as ceramic balls. This setup provides uniform lighting that originates from the camera's perspective, effectively reducing shadows caused by surface irregularities and minimizing light interference. Moreover, it significantly enhances image contrast and clarity, making the details more pronounced and facilitating more accurate visual inspections and measurements. As illustrated in Fig. 2, taking the erosion defect as an example, sample collected without a coaxial light source suffers from a significant environmental and lighting interference and exhibits shadows. In contrast, sample collected with a coaxial light source displays no shadows and is minimally affected by external conditions.

To ensure the diversity and comprehensiveness of the data, this paper collected the various typical defects of both black (Si_3N_4) and white (ZrO_2) ceramic balls. Pit defects are predominantly found in black ceramic balls, whereas scratches, porosity, and erosion types of defects are more common in white ceramic balls. The experiments employed a colour COMS camera (GS3-U3-51S5C-C, FLIR) to capture images of these defects under varying light conditions, simulating the lighting scenarios likely to be encountered in a real factory setting. The images of the defective ceramic balls, as shown in Fig. 3, reveal that the surface defects are small and the contrast is low. In images of pit defects, localized tissue spalling with distinct edges is clearly visible. Scratch defects appear as elongated, linear marks, while porosity and erosion defects present as dots or point-like formations.

(a) (b)

Fig. 2. The collected defective ceramic ball sample images.
(a) using coaxial light source; (b) without using coaxial light source.

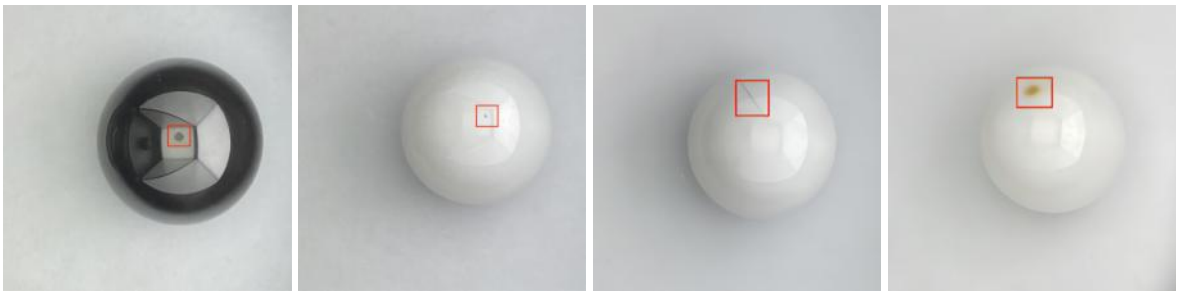

(a) pit (b) pore (c) scratch (d) erosion
Fig. 3. Ceramic ball surface typical defects images.

A total of 1027 samples of ceramic balls were collected, and 384 samples of ceramic balls were obtained by filtering out invalid images, such as blurred and duplicated images. Neural network training requires a lot of input samples to avoid model failure to converge and overfitting problems. Insufficient samples may cause the model to learn noise and fall into local optimum, making it difficult to evaluate the model performance. Therefore, image enhancement techniques become especially critical.

2.2. Date Enhancement

To avoid potential issues such as overfitting, data augmentation is necessary for the dataset. In digital image processing, histogram equalization [20-22] is a common method to enhance image contrast and visual effects by adjusting the grayscale distribution. However, since this paper focuses on ceramic balls with small defect targets and low contrast, conventional histogram equalization struggles to highlight details and defects effectively. Therefore, the *Contrast Limited Adaptive Histogram Equalization* (CLAHE) [23] algorithm was utilized in this paper to enhance the original images, revealing subtle defect information more effectively. CLAHE, the adaptive histogram equalization algorithm, enhances the details of an image by limiting the contrast.

The image is divided into small blocks called “tiles”. Each tile undergoes independent histogram equalization, allowing for localized enhancement and improving local contrast in each small region of the image. For each tile, its grayscale histogram is denoted as *h(i)*, and the clipping threshold *T* is computed as

$$T = \frac{C_{clip} \times N_x \times N_y}{M}, \tag{1}$$

where C_{clip} is the clipping factor, N_x and N_y are the number of pixels in the width and height of each subgraph, respectively, and *M* is the number of grey levels of the corresponding subgraph. If any *h(i)* in the histogram exceeds the set clipping threshold *T*, the excess pixels *N* are evenly redistributed to other grayscale levels. The number of extra pixels allocated to each grayscale level is N_{ave}

$$N = \sum_{i=0}^{M-1} \{\max[h(i) - T]\}, \tag{2}$$

$$N_{ave} = \frac{N}{M}. \tag{3}$$

This method not only prevents noise amplification, but also smooths the edges of the tiles using bilinear interpolation after equalizing all the tiles, eliminating the obvious boundaries between the tiles, so that the image enhancement shows an overall uniformity and naturalness. As shown in Fig. 4, the grey scale histogram of the sample after using the CLAHE algorithm is more uniform compared to the grey scale histogram of the original image. Through this local equalization and interpolation process, the small target defects in the image are effectively enhanced and are more suitable for human eye observation.

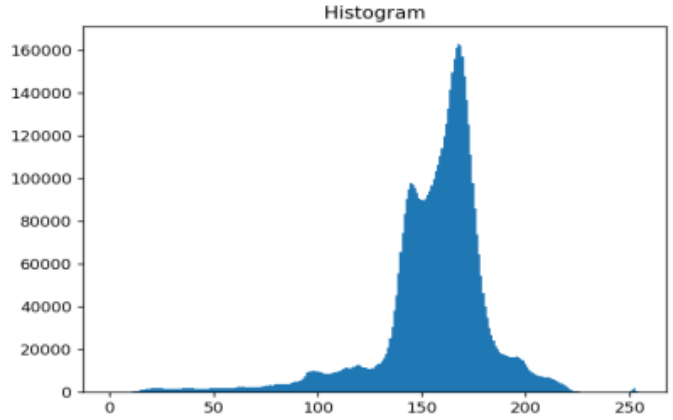

(a)

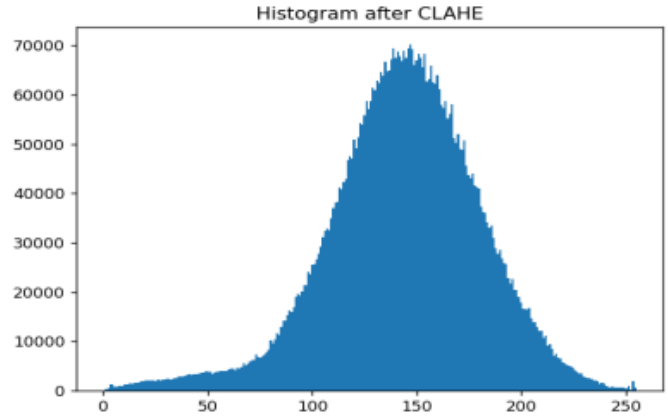

(b)

Fig. 4. Grey scale histogram of samples processed with (a) and without (b) the CLAHE algorithm.

In object detection, a diverse and high-quality dataset is crucial for the performance of neural network models. This study thus employed the median filter to augment the ceramic ball image samples data. Techniques such as changing light intensity, cropping, horizontal flipping, Mosaic, adding Gaussian noise, enhancing contrast, and employing the CLAHE algorithm were used to process images of the collected ceramic ball image dataset with defects. As an example of ablation defects, the images augmentation data are shown in Fig. 5.

(a) original image (b) change light intensity (c) crop size (d) flip horizontally

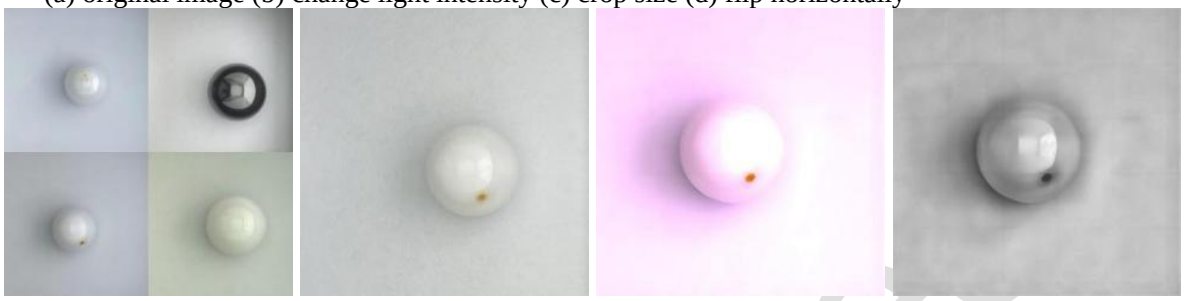

(e) mosaic (f) adding Gaussian noise (g) contrast enhancement (h) CLAHE

Fig. 5. Enhancement images of ceramic ball surface defects.

3. Improvement of YOLOv8

YOLOv8, developed by Ultralytics [24], is the latest deep convolutional neural network based on a single-stage object detection algorithm and represents a continuation of the You Only Look Once series. This model enhances the capabilities of its predecessor, YOLOv5 [25], by optimizing underlying feature extraction and improving semantic and contextual information integration. The enhancements include an optimized backbone network and prediction head, as well as the replacement of all C3 modules in the YOLOv5 network with C2f modules [26], leading to an increased detection accuracy. YOLOv8 shows significant improvements in processing speed and detection accuracy for high-resolution images compared to YOLOv5. Trained on large-scale datasets, the model exhibits excellent generalization capabilities across various object detection tasks. To meet real-time operational requirements, YOLOv8 is designed with fewer parameters. For the specific task of detecting surface defects on ceramic balls, the YOLOv8n network was chosen due to its balance of accuracy and speed. However, challenges such as low detection accuracy and missing detections persist in identifying defects on ceramic ball. Therefore, this study proposes further design improvements for the YOLOv8 model to address these issues.

3.1. Network Modelling Improvements

To enhance detection performance and reduce computational costs, significant improvements and optimizations have been implemented in the following areas. First, to more effectively extract features of target defects, the ADown module has been introduced, replacing the convolutional modules in the YOLOv8 model. This module enhances feature extraction by employing multiple convolution and pooling operations that gradually reduce the size of the feature maps while increasing the number of channels. Second, the loss function has been changed to the Powerful-IoU (*Powerful for Intersection Over Union*) loss function [27]. This modification increases the loss function's capability to handle scenarios with occluded defects or multiple defects, thereby enhancing the model’s learning efficacy. Fig. 6 illustrates the structure of the modified YOLOv8-AP model, which is based on these improvements to the original YOLOv8 framework.

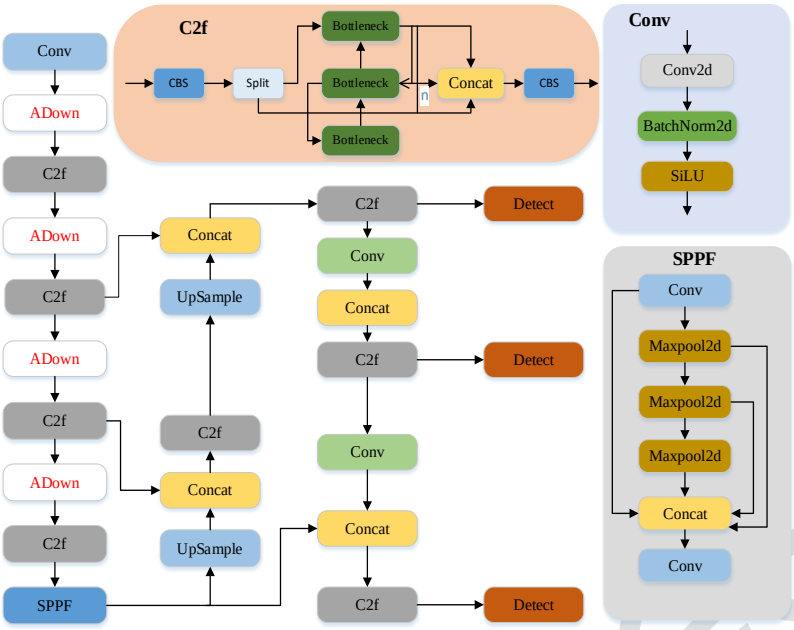

Fig. 6. The improved YOLOv8-AP structure.

3.2. ADown Module

To address the issue of small defect sizes on ceramic balls, most existing techniques employ the traditional FPN (*Feature Pyramid Network*) [28] for feature fusion. This approach transfers high-level, semantically-rich information to lower-level features in a top-down manner. In contrast, the ADown module, a crucial component of YOLOv9, utilizes a multipath processing mechanism to enhance interactions between different levels of features, thus improving the model's ability to detect targets of various sizes. The structure of the ADown module is depicted in Fig. 7. It adopts a lightweight design strategy that significantly reduces the model's complexity by optimizing and minimizing the number of parameters. Unlike traditional down sampling techniques, such as simple pooling layers or conventional convolutional stride adjustments, the ADown module preserves critical target features through finer structural adjustments. This not only enhances the model's efficiency but also allows it to adapt its structure and functionality dynamically to suit different data and application scenarios, effectively overcoming the limitations posed by resource constraints in real-time applications on mobile devices and embedded systems.

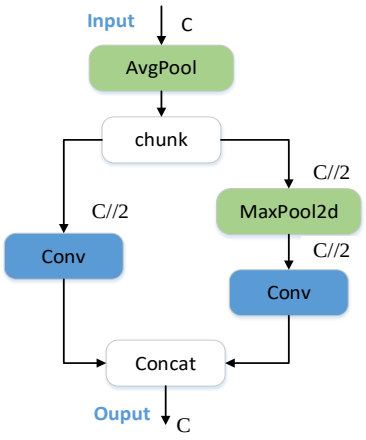

Fig. 7. ADown module structure.

As shown in Fig. 8, in specific, with a kernel size of 2×2, an image with input dimensions of 640×640 is processed through MaxPool2d (maximum pooling), reducing the dimensions of the image by half in each direction, resulting in a feature map of 320×320. The principle of MaxPool2d is illustrated in Figure 8, where the left panel shows the feature values contained within the feature map. The feature map is systematically scanned using a predefined kernel size and stride.

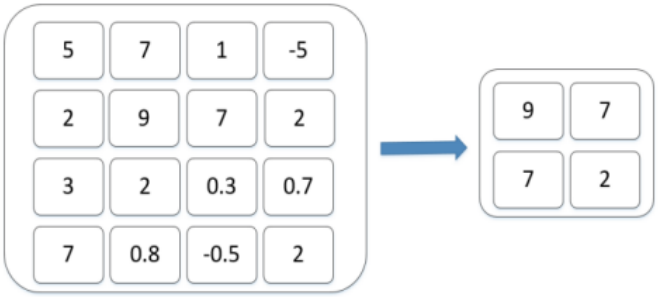

Fig. 8. MaxPool2d schematic.

For each kernel-sized region, this operation picks the maximum value in the region, effectively capturing the most significant features in the local region. When using a 2 × 2 kernel size and corresponding step size, each 2 × 2 block in the input is evaluated and the highest value in each block is retained. The first block is calculated as follows.

$$Output1 = Maximum\ (5,7,2,9) = 9. \tag{4}$$

This method not only reduces the data dimensionality and boosts computational efficiency, but also enhances the invariance of the model to small translations and deformations. After maximum pooling, the feature map is divided into two parts, each maintaining a spatial size of 320×320. Each split feature map is then directed along two separate paths, where they undergo further processing with a second MaxPool2d and CBS (*Combi Brake System*) operations. This second round of MaxPooling halves the dimensions from 320×320 to 160×160 in each direction. Finally, the output size of each pathway is reduced to 80×80. This procedure significantly decreases the spatial size of the feature maps while retaining critical features, thereby reducing computational demands and enhancing the model's detection capabilities. Clearly, the introduction of the ADown module offers an efficient, adjustable, and precise down sampling tool for the detection of surface defects on ceramic ball.

3.3. Powerful-IoU Loss Function

The Powerful-IoU loss function is a technique used to enhance model performance in object detection tasks, particularly in terms of object localization accuracy. This loss function builds upon and refines the traditional IoU (*Intersection over Union*) [29] loss to address its insensitivity in certain scenarios, especially when the predicted bounding box has little or no overlap with the true bounding box. The Powerful-IoU loss function consists of three key components: the IoU term, the centroid distance term C, and the aspect ratio term v. IoU is the intersection and concurrency ratio between the predicted bounding box and the true bounding box, and is an intuitive measure of the similarity of the two bounding boxes. The formulas for the calculation of IoU, C, and v are, respectively, expressed as

$$IoU = \frac{Area\ of\ \ Overlap}{Area\ of\ \ Union}, \tag{5}$$

$$C = \sqrt{(x_2 - x_1)^2 + (y_2 - y_1)^2}\ , \tag{6}$$

$$v = \frac{4}{\pi^2}\left(\tan^{-1}\frac{w_{gt}}{h_{gt}} - \tan^{-1}\frac{w_{pred}}{h_{pred}}\right)^2, \tag{7}$$

where w_{gt}, h_{gt} are the width and height of the real frame, and w_{pred}, h_{pred} are the width and height of the predicted frame. Thus, the formula for Powerful-IoU loss can be written as

$$Powerful\text{ - }IoU\ Loss = 1 - IoU + \frac{\rho^2\left(b, b_{gt}\right)}{C^2} + \alpha v\,, \tag{8}$$

where $\rho(b, b_{gt})$ denotes the Euclidean distance between the center of the predicted frame and the real frame, and is the coefficient used to balance the aspect ratio term, which is usually a fixed parameter. In this way, the Powerful-IoU loss function is not only optimized over the overlapping regions of the predicted and real frames, but also takes their geometries and relative positions into consideration, which helps to improve the localization accuracy. Therefore, Powerful-IoU is an efficient loss function that can significantly improve the localization accuracy in target detection tasks. By addressing some of the limitations in traditional IoU losses, it enables the network to learn more consistently and efficiently in a variety of situations.

4. Experiments

4.1. Data Set and Experimental Environment

In this study, different lighting intensities were simulated by adjusting the light source controller. Images were captured using a COMS industrial camera at a resolution of 2024×2024 pixels and saved in PNG format. A total of 1,027 ceramic ball samples were collected, featuring four types of defects: pits, pores, scratches, and erosions. Data augmentation was applied to 384 well-captured images, resulting in 1,518 effective samples that were subsequently annotated. The dataset was divided into training, testing, and validation sets in a 7:2:1 ratio. Each type of defect was labelled and visually experimented, as shown in Fig. 9. Each matrix cell represents a label used during model training, and the depth of the region colour reflects the correlation between respective labels. Darker areas indicate a deeper understanding of the correlation between these two labels by the model, whereas lighter areas indicate weaker correlations.

Fig. 9 (a) shows a histogram of the number of categories in the dataset. Fig. 9 (b) details the distribution of labels in the original dataset. Analysis reveals that the distribution of defects in the self-built dataset is uneven. The accuracy of the rectangular bounding boxes indicates that this method is suitable for detecting surface defects on ceramic balls.

The experiments were implemented under the PyTorch deep learning framework and use a single RTX 3090 graphics card for model training. The specific configuration of the experimental environment is shown in Table 1.

Table 1. Experimental environment.

Name of the environment	Name
operating system	Ubuntu 20.04
GPUs	RTX3090
CPU	Intel(R) Xeon(R) Platinum 8362 CPU @ 2.80GHz
RAM	24GB
Deep learning frameworks	PyTorch (1.11.0)
Interpreter	Python (3.8)
CUDA version	CUDA (11.3)

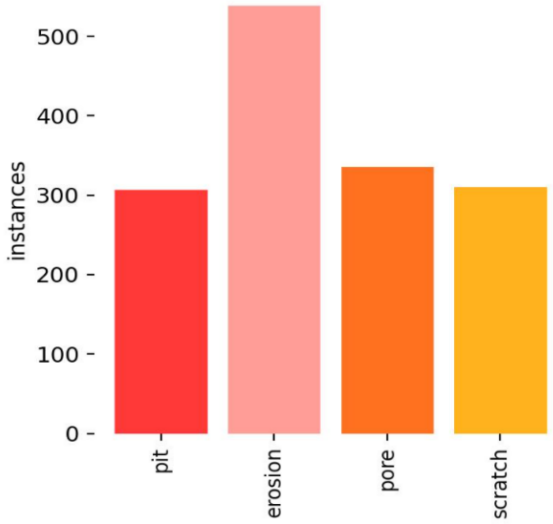

(a) distribution of dataset categories

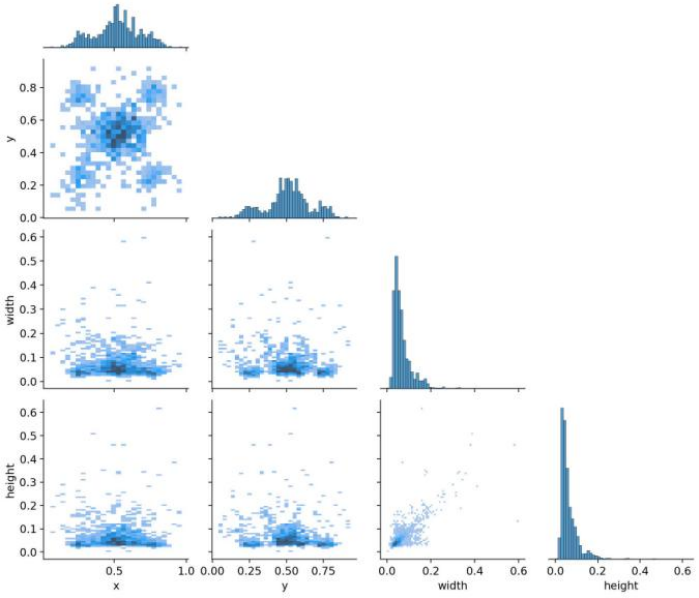

(b) details of label distribution

Fig. 9. Statistics and visualization of annotated files of the dataset.

4.2. Evaluation Indicators

To comprehensively evaluate the performance of the YOLOv8 network model, this paper employed several key metrics, including Recall, Precision, multi-class average accuracy (mAP0.5), detection speed, and number of parameters. mAP0.5 represents the average accuracy under different confidence thresholds, and it is an important metric for evaluating the accuracy of multi-class target detection. In addition, the detection speed of the model is quantified by the number of *frames per second* (FPS) processed, which examines the response speed and processing efficiency of the model in practical applications. The performance calculation is based on (9) to (13)

$$Precision = \frac{T_p}{T_p + F_p}, \tag{9}$$

$$Recall = \frac{T_p}{T_p + F_N}, \tag{10}$$

$$F_1 = 2 \times \frac{Precision \times Recall}{Precision + Recall}, \tag{11}$$

$$AP = \int_0^1 Precision(Recall) d_{Recall}, \tag{12}$$

$$mAP = \frac{\sum_{i=1}^{C} AP(i)}{C}. \tag{13}$$

In the above equations, T_p indicates that the positive samples predicted by the model are in the positive category, F_p indicates that the negative samples predicted by the model are in the positive category, and F_N indicates that the positive samples predicted by the model are in the negative category, so as to ensure the accuracy and reliability of the assessment results.

4.3. Experimental Results

4.3.1. Influence of Different Backbone Networks on the Model

In this study, the YOLOv8n object detection network serves as the foundational model, with the introduction of the ADown module to replace the convolutional modules within the YOLOv8 framework. This substitution incorporates commonly used lightweight feature extraction backbone networks such as the CBAM module (*Convolutional Block Attention Module*) [30], CA module (*Coordinate Attention*) [31], and DAT module (Vision Transformer with Deformable Attention) [32]. Keeping all parameters consistent except for the backbone network, the experimental results listed in Table 2 illustrate varied training outcomes among the different backbone networks. Compared to the CA, DAT, and CBAM networks, the ADown-enhanced approach exhibits higher training accuracy, recall, and mean average precision. Relative to the other networks, the mAP0.5 scores have increased by 3.1%, 0.9%, and 1.7%, respectively. Therefore, the ADown module significantly improves the detection performance of the YOLOv8 model.

Table 2. Performance comparison of different backbone networks.

Models	**Backbone network**	**Precision /%**	**Recall rate /%**	**mAP0.5 /%**	**mAP0.5-0.95 /%**	**Number of parameters /M**	**FLOPs /G**
YOLOv8	CBAM	93.0	91.4	93.0	45.7	3.0	7.4
YOLOv8	CA	94.2	93.3	95.2	46.9	3.0	8.1
YOLOv8	DAT	92.8	92.7	94.4	43.3	2.7	7.5
YOLOv8	ADown	94.8	93.5	96.1	47.4	2.7	7.5

4.3.2. Ablation Experiments

This study implemented two key enhancements in the YOLOv8 model to boost its performance. Firstly, the introduction of the ADown module replaced the original convolution modules to optimize the model structure. Secondly, the Powerful-IoU loss function was adopted

in place of the traditional loss functions to enhance detection precision. To assess the actual effects of these improvements, a series of ablation experiments were conducted. The results, shown in Table 3, indicate that with the YOLOv8n model unchanged, the integration of the ADown module alone resulted in the YOLOv8-A model having a 10% reduction in the number of parameters, with recall and mAP0.5 increasing by 1% and 2.7%, respectively. Replacing only the loss function with Powerful-IoU in the YOLOv8-P model maintained the parameter count while improving mAP0.5 by 1.8%. Lastly, by introducing the ADown module and replacing the loss function, the YOLOv8-AP model was achieved. This model, without an increase in parameter volume, further improved in recall and mAP0.5, demonstrating enhanced detection capabilities for surface defects in ceramic balls.

Table 3. Results of ablation experiments.

Models	Precision /%	Recall rate /%	mAP0.5 /%	mAP0.5-0.95 /%	Number of parameters /M	FLOPs /G
YOLOv8n	90.6	92.5	93.4	47.5	3.0	8.1
YOLOv8-A	94.8	93.5	96.1	47.4	2.7	7.5
YOLOv8-P	92.1	91.7	95.2	47.6	3.0	8.1
YOLOv8-AP	94.8	94.0	96.1	48.9	2.7	7.5

4.3.3. Performance Comparison of Different Models

To validate the effectiveness of the YOLOv8-AP model for detecting surface defects on ceramic balls, this study conducted comparative training and testing using the YOLOv5s, YOLOv9-c, YOLOv8n, SSD-300 and YOLOv7 models on a dataset of ceramic balls, with performance results presented in Table 4. When compared with the lightweight networks in the YOLO series such as YOLOv5s, YOLOv9-c, YOLOv8n and YOLOv7, the improved YOLOv8-AP model achieved significant performance optimization. Specifically, compared to these models, YOLOv8-AP reduced the parameter count by 61.4%, 94.7%, 10% and 92.7%, respectively, effectively lowering computational demands. In terms of performance evaluation, mAP0.5 improved by 2.2%, 4.8%, 2.7% and 16.9%, respectively, and recall rates also saw varying degrees of enhancement. These results indicate that the YOLOv8-AP algorithm, while maintaining a smaller model size, provides higher detection accuracy and lower computational costs, thereby optimizing detection efficiency. This makes the algorithm not only suitable for real-time object detection of surface defects on ceramic balls but also facilitates deployment and application on resource-limited devices.

Table 4. Performance comparison of different models.

Models	**Model size /MB**	**Recall rate /%**	**mAP0.5 /%**	**Number of parameters /M**	**FLOPs /G**
YOLOv5s	14.5	90.6	93.9	7.0	15.8
YOLOv9-c	102.8	87.4	91.3	50.7	236.7
YOLOv8n	6.3	92.5	93.4	3.0	8.1
SSD-300	100.3	28.75	82.49	102.2	31.0
YOLOv7	74.8	73.2	79.9	37.2	105.2
YOLOv8-AP	5.7	94.0	96.1	2.7	7.5

As illustrated in Fig. 10, the comparison of loss values for the YOLOv5s, YOLOv9-c, YOLOv8n, YOLOv7, SSD-300 and YOLOv8-AP models shows that the YOLOv8-AP model, represented by the red curve, has the smallest loss value. This indicates that the error between the models' predictions and the actual results is minimal, demonstrating a significant improvement in the models' performance.

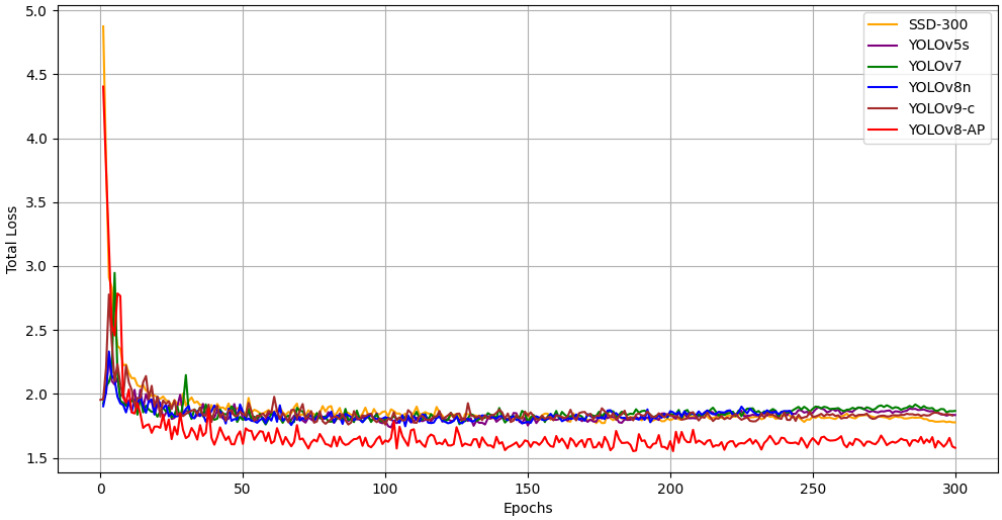

Fig. 10. Comparison of loss values for different models.

4.3.4. Comparison of Detection Accuracy of Different Light Source

To verify the effectiveness of using a coaxial light source for detecting surface defects on ceramic balls, the study collected 240 samples of ceramic ball defects without the coaxial light source. These samples were processed using the same data augmentation methods, resulting in 977 effective images. The dataset was then tested using the improved YOLOv8-AP model. According to Table 5, the results from using the coaxial light source showed improvements in accuracy, recall rate, and mAP0.5 values by 1.3%, 6.9%, and 4.8% respectively, compared to those without the coaxial light source. This experiment demonstrates the effectiveness of the coaxial light source in enhancing the detection of surface defects on ceramic balls.

Table 5. Comparison of detection results with and without coaxial light source.

Light source	**Models**	**Precision /%**	**Recall rate /%**	**mAP0.5 /%**	**FLOPs /G**
Non-coaxial light source	YOLOv8-AP	91.9	87.1	91.3	7.5
Coaxial light source	YOLOv8-AP	93.2	94.0	96.1	8.1

Fig. 11 shows the detection results of surface defects on ceramic balls using the YOLOv8 model under coaxial light, the YOLOv8-AP model under coaxial light, and the YOLOv8-AP model without coaxial light. The experimental results indicate that both models can detect the surface defects on ceramic balls. However, YOLOv8 exhibits issues of low detection precision and missed detections when dealing with smaller target sizes. In contrast, the YOLOv8-AP model demonstrates superior recognition accuracy. Furthermore, when analysing the loss values of the models under different scenarios for detecting ceramic balls, YOLOv8-AP shows a better adaptability to complex environments and consistently records the lowest loss across all conditions. These results completely indicate that YOLOv8-AP has a distinct advantage in ensuring the accuracy and reliability of detection.

(a) (b) (c)

Fig. 11. Detection results of ceramic balls using different models.
(a) YOLOv8 model with coaxial light source; (b) YOLOv8-AP model with coaxial light source; (c) YOLOv8-AP model without coaxial light source.

5. Conclusions

This study innovatively applied the improved YOLOv8-AP model for nondestructive detection of small target defects on ceramic balls. To address the severe specular reflection issues, the coaxial light source was employed, significantly reducing the impact of specular reflection effect on the experiments. Various data augmentation techniques were utilized to enhance model robustness, along with the application of CLAHE to improve image contrast. The ADown module was introduced to improve the performance of YOLOv8 algorithm, which progressively reduced the feature map size while increasing the number of channels through multiple convolutional and pooling operations, thereby more effectively extracting features.

Additionally, the loss function was replaced with the Powerful-IoU loss function, which incorporated adjustable parameters to tackle challenges in multi-target detection and occlusion. Experimental results demonstrate that the improved YOLOv8-AP model achieved a mAP0.5 and recall rate of 96.1% and 94%, respectively, on a custom dataset of surface defects in ceramic balls. Compared to the YOLOv8 algorithm, the mAP0.5 and recall rate were improved by 2.7% and 1.5%, respectively, while the parameter count was reduced by 10%. These findings completely validate the enhancement of the detection efficiency of the improved YOLOv8-AP model in the fields of the detection of ceramic ball defects.

This study not only advances the understanding of small target detection technologies but also provides reliable technical support for industrial practices, particularly in high-precision, intelligent detection of ceramic balls, holding significant practical value. However, despite the excellent performance of the improved YOLOv8-AP model, further testing of ceramic balls by use of the improved YOLOv8-AP model is necessary to enhance robustness under the actual industrial scenarios, which will be the next work to be investigated.

Acknowledgements

This work was supported by Jiangsu Provincial Market Regulation Administration Science and Technology Project (No. KJ2024092) and Lianyungang Major Technology Research Project of Open Bidding for Selecting the Best Candidates (No. CGJBGS2202).

References

[1] Wu, C., Liu, Z., Zhao, H., Yang, H., Li, X., & Ni, J. (2023). Effect of the grease thickener on tribological properties of Si3N4/GCr15 contact interface and the performance in hybrid ceramic ball bearing. *Ceramics International*, *49*(11), 16857–16867. https://doi.org/10.1016/j.ceramint.2023.02.047

[2] Wen, D. S., Wang, S. R., Wang, G. Q., Guo, P. Q., Yang, L. Y., & Yang, X. F. (2018). Fabrication processing and mechanical properties of Si_3N_4 ceramic turbocharger wheel. *Ceramics International*, *44*(9), 10596-10603. https://doi.org/10.1016/j.ceramint.2018.03.084

[3] Liang, H. Q., Zeng, Y. P., Zuo, K. H., Xia, X. F., Yao, D. X., & Yin, J. W. (2017). The effect of oxidation on the mechanical properties and dielectric properties of porous Si_3N_4 ceramic. *Ceramics International*, *43*(7), 5517-5523. https://doi.org/10.1016/j.ceramint.2017.01.074

[4] Fekri-Ershad, S., & Tajeripour, F. (2017). Multi-Resolution and Noise-Resistant Surface Defect Detection Approach Using New Version of Local Binary Patterns. *Applied Artificial Intelligence*, *31*(5–6), 395–410. https://doi.org/10.1080/08839514.2017.1378012

[5] Xing, H., Zou, B., Liu, X., Wang, X., Huang, C., & Hu, Y. (2020). Fabrication strategy of complicated Al2O3-Si3N4 functionally graded materials by stereolithography 3D printing. *Journal of the European Ceramic Society*, *40*(15), 5797–5809. https://doi.org/10.1016/j.jeurceramsoc.2020.05.022

[6] Yu, D., Zhu, Z., Min, J., Fang, C., Liao, D., & Wu, N. (2020). Multi-scale decomposition enhancement algorithm for surface defect images of Si_3N_4 ceramic bearing balls based on stationary wavelet transform. *Advances in Applied Ceramics*, *120*(1), 47–57. https://doi.org/10.1080/17436753.2020.1858010

[7] Ding, Y., Zhang, X., & Kovacevic, R. (2016). A laser-based machine vision measurement system for laser forming. *Measurement*, *82*, 345–354. https://doi.org/10.1016/j.measurement.2015.10.036

[8] Deneuville, F., Duquennoy, M., Ouaftouh; Ourak, M., Jenot, F., & Desvaux, S. (2009). High frequency ultrasonic detection of C-crack defects in silicon nitride bearing balls. *Ultrasonics*, *49*(1), 89-93. https://doi.org/10.1016/j.ultras.2008.06.010

[9] Li, X., Chen, L., Liu, S., Shao, M., Hu, R., Li, R., Li, Y., & An, D. (2024). A method for multi-view surface defect detection of Si_3N_4 ceramic bearing balls integrating features enhanced by the Gabor salient domain. *Measurement Science and Technology*, *35*(8), 085205. https://doi.org/10.1088/1361-6501/ad4812

[10] Zhang, K., Fu, L., Wang, Z., Sun, Y., & Liu, C. (2017). Research on surface defect detection of ceramic ball based on fringe reflection. *Optical Engineering*, *56*(10), 1. https://doi.org/10.1117/1.oe.56.10.104104

[11] Yu, D., Zhang, H., Zhang, X., Liao, D., & Wu, N. (2021). Si3N4 Ceramic Ball Surface Defects' Detection Based on SWT and Nonlinear Enhancement. *Mathematical Problems in Engineering*, *2021*, 1–9. https://doi.org/10.1155/2021/4922315

[12] Chen, S., Wang, D.-G., & Wang, F.-B. (2022). Detecting aluminium tube surface defects by using faster region-based convolutional neural networks. *Journal of Computational Methods in Sciences and Engineering*, *22*(5), 1711–1720. https://doi.org/10.3233/jcm-226107

[13] Liao, D., Cui, Z., Zhu, Z., Jiang, Z., Zheng, Q., & Wu, N. (2023). A nondestructive recognition and classification method for detecting surface defects of Si3N4 bearing balls based on an optimized convolutional neural network. *Optical Materials*, *136*, 113401. https://doi.org/10.1016/j.optmat.2022.113401

[14] Fan, Y. B., Mao, S. J., Li, M., Wu, Z., & Kang, J. T. (2024). CM-YOLOv8: Lightweight YOLO for Coal Mine Fully Mechanized Mining Face. *Sensors*, *24*(6), 1866. https://doi.org/10.3390/s24061866

[15] Lv, X., Yi, H. A., Fang, R. J., Ai, S. H., & Lu, E. H. (2023). Visual detection of milling surface roughness based on improved YOLOv5. *Metrology and Measurement Systems*, *30*(3), 531-548. https://doi.org/10.24425/mms.2023.146425

[16] Zhu, F., Chang, C., Li, Z. H., Li, B. Q., & Li, L. (2024). A generic optimization-based enhancement method for trajectory data: Two plus one. *Accident Analysis & Prevention*, *200*, 107532. https://doi.org/10.1016/j.aap.2024.107532

[17] Katsampiris-Salgado, K., Dimitropoulos, N., Gkrizis, C., Michalos, G., & Makris, S. (2024). Advancing human-robot collaboration: Predicting operator trajectories through AI and infrared imaging. *Journal of Manufacturing Systems*, *74*, 980–994. https://doi.org/10.1016/j.jmsy.2024.05.015

[18] Wu, X., Ouyang, G., Li, B., Cui, L., & Zhou, G. (2020). Determining Line-Crossing Sequences Between Laser Printing and Writing Pen Using Coaxial Light. *Journal of Forensic Sciences*, *65*(4), 1242–1246. https://doi.org/10.1111/1556-4029.14316

[19] Chen, S. (2016). Inspecting lens collars for defects using discrete cosine transformation based on an image restoration scheme. *IET Image Process.*, *10*(6), 474-482. https://doi.org/10.1049/iet-ipr.2015.0780

[20] Hejazi, A. S., Al-Hunaiti, A. H., Bsoul, I., Mohaidat, Q., & Mahmood, S. H. (2024). Optimizing the synthesis of $ZnFe_2O_4$ through chemical and physical methods: effects of the synthesis route on the phase purity, inversion, and magnetic properties of spinel zinc ferrite. *Physica Scripta*, *99*(6), 065029. https://doi.org/10.1088/1402-4896/ad4746

[21] Sokhan', S. V., Maystrenko, A. L., Borimsky, A. I., Voznyy, V. V., Sorochenko, V. G., Hamaniuk, M. P., & Zubaniev, E. M. (2021). Changing the Performance of Diamond Finishing of Ceramic Balls of Boron Carbide and Silicon Nitride. *Journal of Superhard Materials*, *43*(2), 135–144. https://doi.org/10.3103/s106345762102009x

[22] Dua, M., Nalawade, S., & Dua, S. (2024). Underwater image enhancement by using amalgamation of colour correction, contrast-enhancing and dehazing. *Physica Scripta*, *99*(4), 046002. https://doi.org/10.1088/1402-4896/ad2d9c

[23] He, Z., Mo, H., Xiao, Y., Cui, G., Wang, P., & Jia, L. (2024). Multi-scale fusion for image enhancement in shield tunneling: a combined MSRCR and CLAHE approach. *Measurement Science and Technology*, *35*(5), 056112. https://doi.org/10.1088/1361-6501/ad25e4

[24] Ding, P., Zhan, H., Yu, J., & Wang, R. (2024). A bearing surface defect detection method based on multi-attention mechanism Yolov8. *Measurement Science and Technology*, *35*(8), 086003. https://doi.org/10.1088/1361-6501/ad4386

[25] Li, A. J., Xu, G. P., Yue, W. P., Xu, C. Y., Gong, C. P., & Cao, J. P. (2024). Object Detection in Hazy Environments, Based on an All-in-One Dehazing Network and the YOLOv5 Algorithm. *Electronics*, 13(10), 1862. https://doi.org/10.3390/electronics13101862

[26] Xiao, B., Nguyen, M., & Yan, W. Q. (2023). Fruit ripeness identification using YOLOv8 model. *Multimedia Tools and Applications*, *83*(9), 28039–28056. https://doi.org/10.1007/s11042-023-16570-9

[27] Liu, C., Wang, K., Li, Q., Zhao, F., Zhao, K., & Ma, H. (2024). Powerful-IoU: More straightforward and faster bounding box regression loss with a nonmonotonic focusing mechanism. *Neural Networks*, *170*, 276–284. https://doi.org/10.1016/j.neunet.2023.11.041

[28] Sharen, H., Jawahar, M., Jani Anbarasi, L., Ravi, V., Saleh Alghamdi, N., & Suliman, W. (2024). FDUM-Net: An enhanced FPN and U-Net architecture for skin lesion segmentation. *Biomedical Signal Processing and Control*, *91*, 106037. https://doi.org/10.1016/j.bspc.2024.106037

[29] Sun, S., Mo, B., Xu, J., Li, D., Zhao, J., & Han, S. (2024). Multi-YOLOv8: An infrared moving small object detection model based on YOLOv8 for air vehicle. *Neurocomputing*, *588*, 127685. https://doi.org/10.1016/j.neucom.2024.127685

[30] Lei, D., Dong, C., Guo, H., Ma, P., Liu, H., Bao, N., Kang, H., Chen, X., & Wu, Y. (2024). A fused multi-subfrequency bands and CBAM SSVEP-BCI classification method based on convolutional neural network. *Scientific Reports*, *14*(1). https://doi.org/10.1038/s41598-024-59348-1

[31] Huo, Y., Gang, S., Dong, L., & Guan, C. (2024). An Efficient Semantic Segmentation Method for Remote-Sensing Imagery Using Improved Coordinate Attention. *Applied Sciences*, *14*(10), 4075. https://doi.org/10.3390/app14104075

[32] Yang, B., Zhang, B., Han, Y., Liu, B., Hu, J., & Jin, Y. (2024). Vision transformer-based visual language understanding of the construction process. *Alexandria Engineering Journal*, *99*, 242–256. https://doi.org/10.1016/j.aej.2024.05.015

Metrol. Meas. Syst., Vol. 32 (2025), No. 1
DOI: 10.24425/mms.2025.152777

Guoqing Gu received the Ph.D, degree from Nanjing University of Aeronautics & Astronautics, China, in 2013. He is currently an Associate Professor of the School of Civil Engineering of Yancheng Institute of Technology. His research activity focuses on experimental mechanics.

Hanlei Wang received the B.Sc, degree from Yancheng Institute Of Technology, China, in 2021. She is a full-time graduate student in Yancheng Institute of Technology, major in mechanical automation, mainly focus on defect detection.

Xuyi Miao received the B.Sc, degree from Yancheng Institute of Technology, China, in 2022. He is a full- time graduate student in Yancheng Institute of Technology, major in system and automatic control, mainly focus on defect detecting.

Jingyi Yan received the M.S. degree in Mechanical Engineering from Carnegie Mellon University, USA, in 2013. His research focuses on the structural development and applications of high-performance alumina, silicon nitride, and zirconia ceramics.

Jianzhou Du received the Ph.D. degree from Nanjing University of Aeronautics and Astronautics, China, in 2014. He is currently an Associate Professor of the School of Materials Science and Engineering, Yancheng Institute of Technology. His research focuses on advanced ceramics and structures.